Human Molecular Genetics, 2015, Vol. 24, No. 13 3708–3717

doi: 10.1093/hmg/ddv115
Advance Access Publication Date: 3 April 2015
Original Article

ORIGINAL ARTICLE

Mutations in *XRCC4* cause primary microcephaly, short stature and increased genomic instability

Nadine Rosin[1,2,3], Nursel H. Elcioglu[5], Filippo Beleggia[1,2,3], Pinar Isgüven[6], Janine Altmüller[1,4], Holger Thiele[4], Katharina Steindl[7], Pascal Joset[7], Anita Rauch[7], Peter Nürnberg[2,3,4], Bernd Wollnik[1,2,3,*] and Gökhan Yigit[1,2,3]

[1]Institute of Human Genetics, [2]Center for Molecular Medicine Cologne (CMMC), [3]Cologne Excellence Cluster on Cellular Stress Responses in Aging-Associated Diseases (CECAD) and [4]Cologne Center for Genomics, University of Cologne, Cologne, Germany, [5]Department of Pediatric Genetics, Marmara University School of Medicine, Istanbul, Turkey, [6]Department of Pediatric Endocrinology, Sakarya University Medical Faculty, Sakarya, Turkey and [7]Institute of Medical Genetics, University of Zurich, Zurich-Schlieren, Switzerland

*To whom correspondence should be addressed at: Institute of Human Genetics, University of Cologne, Kerpener Str. 34, 50931 Cologne, Germany. Tel: +49 22147886817; Fax: +49 22147886812; Email: bwollnik@uni-koeln.de

Abstract

DNA double-strand breaks (DSBs) are highly toxic lesions, which, if not properly repaired, can give rise to genomic instability. Non-homologous end-joining (NHEJ), a well-orchestrated, multistep process involving numerous proteins essential for cell viability, represents one major pathway to repair DSBs in mammalian cells, and mutations in different NHEJ components have been described in microcephalic syndromes associated, e.g. with short stature, facial dysmorphism and immune dysfunction. By using whole-exome sequencing, we now identified in three affected brothers of a consanguineous Turkish family a homozygous mutation, c.482G>A, in the *XRCC4* gene encoding a crucial component of the NHEJ pathway. Moreover, we found one additional patient of Swiss origin carrying the compound heterozygous mutations c.25delG (p.His9Thrfs*8) and c.823C>T (p.Arg275*) in *XRCC4*. The clinical phenotype presented in these patients was characterized by severe microcephaly, facial dysmorphism and short stature, but they did not show a recognizable immunological phenotype. We showed that the *XRCC4* c.482G>A mutation, which affects the last nucleotide of exon 4, induces defective splicing of *XRCC4* pre-mRNA mainly resulting in premature protein truncation and most likely loss of XRCC4 function. Moreover, we observed on cellular level that XRCC4 deficiency leads to hypersensitivity to DSB-inducing agents and defective DSB repair, which results in increased cell death after exposure to genotoxic agents. Taken together, our data provide evidence that autosomal recessive mutations in *XRCC4* induce increased genomic instability and cause a NHEJ-related syndrome defined by facial dysmorphism, primary microcephaly and short stature.

Introduction

Maintenance of genomic integrity and the protection of DNA against damage are important processes required for proper cell function and survival. DNA damage can be caused by different endogenous factors such as replication stress during proliferation or reactive metabolites as well as by exposure to exogenous factors such as UV light, radiation or mutagenic chemicals, and it affects both proliferating and non-dividing, differentiated cells. As the accumulation of DNA damage has an important impact on cell viability, organisms have evolved various mechanisms to protect the integrity of DNA by inducing DNA damage responses or triggering cell death. Among the different types of

Received: December 29, 2014. **Revised:** February 24, 2015. **Accepted:** March 30, 2015

DNA damage, double-strand breaks (DSBs) belong to the most cytotoxic and deleterious types, and two major DSB repair pathways are known to sense double-strand lesions and restore DNA integrity: homologous recombination (HR) and non-homologous end-joining (NHEJ) (1). HR is considered to be the more accurate mechanism to repair DSBs, but it requires the presence of a proper template to exchange and replace defective genetic information (2). In contrast, NHEJ is generally considered to be more prone to errors, but does not rely on a homologous template like, e.g. sister chromatids (3,4). Whether HR or NHEJ is activated to repair DSBs is mainly determined by the cell type, the cell cycle phase and the DNA structure at the site of DNA break (5).

Several human congenital syndromes have been described that are associated with defects in components involved in NHEJ. These include mutations in the catalytic subunit of the DNA-activated protein kinase (DNA-PKcs; encoded by *PRKDC*, MIM 6 00 899) gene encoding the catalytic subunit of a nuclear DNA-dependent serine/threonine protein kinase, which binds to DNA DSBs and facilitates recruitment of other proteins to the lesion, in the non-homologous end-joining factor 1 gene (*NHEJ1*, MIM 6 11 290; also known as *XLF* and *Cernunnos*) and in the DNA cross-link repair protein 1C (*DCLRE1C*, MIM 6 05 988; also known as *Artemis*) gene. Furthermore, several mutations in the DNA ligase IV gene (*LIG4*, MIM 6 01 837) have been identified, encoding an ATP-dependent DNA ligase that catalyses the final DNA ligation step and is crucial for efficient joining of DNA strands in NHEJ (6–11). Individuals with autosomal recessive mutations in these genes mainly present with severe immunodeficiency due to defective V(D)J recombination during lymphocyte development, a process depending on NHEJ, and show additional characteristics like primary microcephaly, short stature and facial dysmorphism. Very recently, it has been proposed that a homozygous missense mutation in *XRCC4* causes severe microcephaly and short stature, but since two other homozygous variants in other genes were also present in this patient, the final proof that recessive *XRCC4* mutations are associated with a microcephalic short-stature syndrome awaits confirmation (12). XRCC4 forms a stable complex with LIG4 during the repair of DNA DSBs by NHEJ, and it has been shown that XRCC4 directly influences the joining activity of LIG4 (13–16).

In this study, we report the identification of novel homozygous and compound heterozygous mutations in *XRCC4* in a Turkish family with three affected children and an individual of Swiss origin presenting with short stature, microcephaly and intellectual disability, and we show that disruption of *XRCC4* induces hypersensitivity to DSBs, defective DNA DSB repair and increased apoptosis after DNA damage.

Results

Clinical characteristics

The Turkish family FAM-01 was referred for genetic counselling due to a congenital, likely autosomal recessive disorder in three brothers born to consanguineous parents, who presented with developmental delay, mild intellectual disability, pronounced primary microcephaly and short stature. The clinical details of the affected individuals are listed in Table 1. The affected brothers also showed a typical facial gestalt characterized by a long, beaked nose, mid-facial hypoplasia and mild hypotelorism (Fig. 1A). At the last referral to the hospital, the brothers were 14 years of age (individual IV.1), 10.5 years of age (IV.2) and 6 months (IV.3). Head circumferences were −7.5 SD (IV.1), −6.5 SD (IV.2) and −4.5 SD (IV.3) and height was also reduced in all three sibs ranging from −3 to −5 SD (Table 1). MRI was available from patient IV.1 and showed a simplified gyral pattern. In addition, the two oldest sibs showed mild thrombocytopenia, but no additional hematological abnormalities. No recurrent infections or other signs for immunological problems were observed in any of the affected individuals.

The index patient II.2 of family FAM-02 is the second child of non-consanguineous Swiss parents and was born spontaneously after an uneventful pregnancy at 38 weeks of gestation. Family history was unremarkable. Early motor milestones were normal but speech development was mildly delayed. Short stature and microcephaly were present from birth (Table 1; Fig. 2A and B). The anterior fontanel was very small at birth (1 × 1 cm) and was found closed at the age of 15 months. Bone age corresponded to the chronological age at 10 years. Apart from malposition of teeth, mild developmental delay and special education mainly due to dyscalculia, clinical course was unremarkable. There was no history of recurrent infections or vegetative problems. Karyotyping after GTG banding and subtelomeric FISH studies revealed normal results.

Identification of homozygous and compound heterozygous XRCC4 mutations

We performed whole-exome sequencing (WES) on DNA extracted from blood lymphocytes of individual IV.1 of family FAM-01 using the NimbleGen SeqCap EZ Human Exome Library v2.0 enrichment kit on an Illumina HiSeq2000 sequencer. WES data analysis and filtering of variants were carried out using the exome analysis pipeline 'Varbank' of the Cologne Center for Genomics (CCG, University of Cologne, Germany) and we obtained a mean coverage of 106 reads, and 96.5% of targets were covered more than 10×. After exclusion of homozygous or compound heterozygous variants in any of the 13 OMIM-referenced genes associated with autosomal recessive isolated or syndromic forms of primary microcephaly, we applied the following criteria for filtering of the WES variants: coverage of more than six reads, a minimum quality score of 10, an allele frequency ≥75%, a minor allele frequency (MAF) <0.5% in the 1000 Genomes database and the Exome Variant Server (EVS; NHLBI Exome Sequencing Project) and not annotated in the in-house WES data sets of the CCG.

Using these filter criteria, we identified in total 16 homozygous variants, 12 of them embedded in the 10 largest homozygous regions (>8 Mb) determined from the WES data set. These homozygous variants included four intronic variants predicted to have minor to none influence on the adjacent splice-sites by different splicing prediction programs, and 12 homozygous missense variants. Among these, only a single homozygous variant was predicted to have a severe impact on protein function and to be most likely deleterious. This variant, c.482G>A, was located at the last nucleotide of exon 4 of the XRCC4 gene, and bioinformatic analysis indicated that the G>A substitution has a severe impact on the proper recognition of the adjacent donor splice-site.

The *XRCC4* gene is embedded within a large homozygous stretch of 21.2 Mb (located between positions chr5:73 931 246 and chr5:95 128 742) and the c.482G>A variant is predicted to completely disrupt the donor splice-site of intron 4 of *XRCC4*. We confirmed the presence of the homozygous variant in patient IV.1 as well as in the two siblings IV.2 and IV.3 by Sanger sequencing and showed that both parents are heterozygous carriers (Fig. 1B). Subsequent analysis of microsatellite markers in all family members confirmed homozygous haplotypes for the identified region on chromosome 5 in all affected individuals (Fig. 1C). Furthermore, the c.482G>A variant is not annotated in

Table 1. Clinical findings in individuals carrying the homozygous and compound heterozygous *XRCC4* mutations compared with individuals with LIG4 syndrome described by Murray *et al.* (11)

Patient	IV.1 (FAM-01)	IV.2 (FAM-01)	IV.3 (FAM-01)	II.2 (FAM-02)	LIG4 patients
Sex	Male	Male	Male	Female	
Mutation	*XRCC4* c.482G>A	*XRCC4* c.482G>A	*XRCC4* c.482G>A	*XRCC4* c.25delC, c.823C>T	*LIG4* various mutations
Gest^{n}/weeks	40	40	40	38	32 to 40
Birth weight	−5.3 SD	−2.8 SD	−2.4 SD	−3.5 SD	−3.0 ± 0.93 SD
Birth OFC	<−3 SD	<−3 SD	<−3 SD	−3.7 SD	−3.6 SD ± 1.37 SD
Birth length	−2 SD	Unknown	Unknown	−2.8 SD	−3.8 ± 1.88 SD
Age at last examination	14 years	10.5 years	6 months	14 years 10 months	—
OFC/SD	−7.5 SD	−6.5 SD	−4.5 SD	−5.0 SD	−10.1 ± 0.95 SD
Height/SD	−5 SD	−5 SD	−3 SD	−2.6 SD	−5.1 ± 1.62 SD
Developmental delay	Mild	Mild	Unknown	Mild	None to moderate
Developmental milestones	Sitting at 6 months walking at 12 months	Unknown	Unknown	Sitting at 6 months, walking at 13 months,	Not described
Intellectual disability	Mild intellectual disability, could not follow primary school, normal daily, practical, social and communication skills	Mild intellectual disability, could not follow primary school, normal daily, practical, social and communication skills	Mild intellectual disability (no details known)	Special education due to dyscalculia; ability to read and write; normal adaptive functioning with personal independence, normal daily, practical, social and communication skills	Unknown
Speech development	Delayed, starting single words at 4 years	Unknown	Unknown	Delayed, first words at 2.6 years	Unknown
Hematological findings	Mild thrombocytopenia (PLT 285.000, age 3 PLT 120.000, age 14)	Mild thrombocytopenia (PLT 133.000, age 10)	Unknown	Not noted	Pancytopenia (onset 2–15 years) marked thrombocytopenia
Immune dysfunction	Not noted	Not noted	Not noted	Not noted	Hypo-/ agammaglobulinemia
Facial dysmorphism & Additional features	Long face with prominent chin, long and beaked nose, high nasal bridge, sloping forehead, mild hypotelorism	Long face with prominent chin, long and beaked nose, high nasal bridge, sloping forehead, mild hypotelorism, undescended testes	Beaked nose, high nasal bridge, sloping forehead, inguinal hernia	Long face with prominent chin, prominent and long philtrum, prominent columella, high nasal bridge, deep set eyes, mild strabism, high forehead, long neck, malpositioning of teeth, excessive white lines on palms, mild truncal obesity	wide nasal bridge, broad nasal tip and a prominent chin, sloping forehead, fine sparse hair
MRI findings	Simplified gyral pattern	Unknown	Unknown	Not performed	Unknown

any current database of human genetic variations including the 1000 Genomes Database, the Exome Variant Server [EVS, National Heart, Lung and Blood Institute Exome Sequencing Project (ESP), Seattle, WA, USA] and the >120 000 alleles of the Exome Aggregation Consortium [Exome Aggregation Consortium (ExAC), Cambridge, MA, USA] indicating that this is most likely the causative mutation in the patients.

Additionally, we performed NGS-based sequencing of 4813 disease-associated genes on DNA extracted from blood lymphocytes of the index patient II.2 of family FAM-02 using the TruSight™ One Sequencing Panel on an Illumina HiSeq System. We obtained an average depth of coverage of 145 reads and 94.2% of the targeted bases were assessed by ≥20 independent sequence reads, and we identified two heterozygous variants, c.25delC (chr5:82 400 762) and c.823C>T (chr5:82 554 426), in *XRCC4*. Sanger sequencing confirmed both mutations in patient II.2 and revealed that parents were each heterozygous carriers for one of these mutations: the c.25delC mutation was paternally inherited, and the c.823C>T mutation was inherited from the mother (Fig. 2C). The c.25delC mutation is predicted to cause a frameshift resulting in a severely truncated protein (p.His9Thrfs*8), whereas the c.823C>T mutation introduces a premature stop codon (p.Arg275*) in *XRCC4*.

The exonic c.482G>A mutation in XRCC4 affects pre-mRNA splicing and protein stability

As the c.482G>A mutation identified in family FAM-01 was predicted to alter splicing of *XRCC4* exon 4, we analyzed the effect of this mutation on the *XRCC4* transcript by RT–PCR and

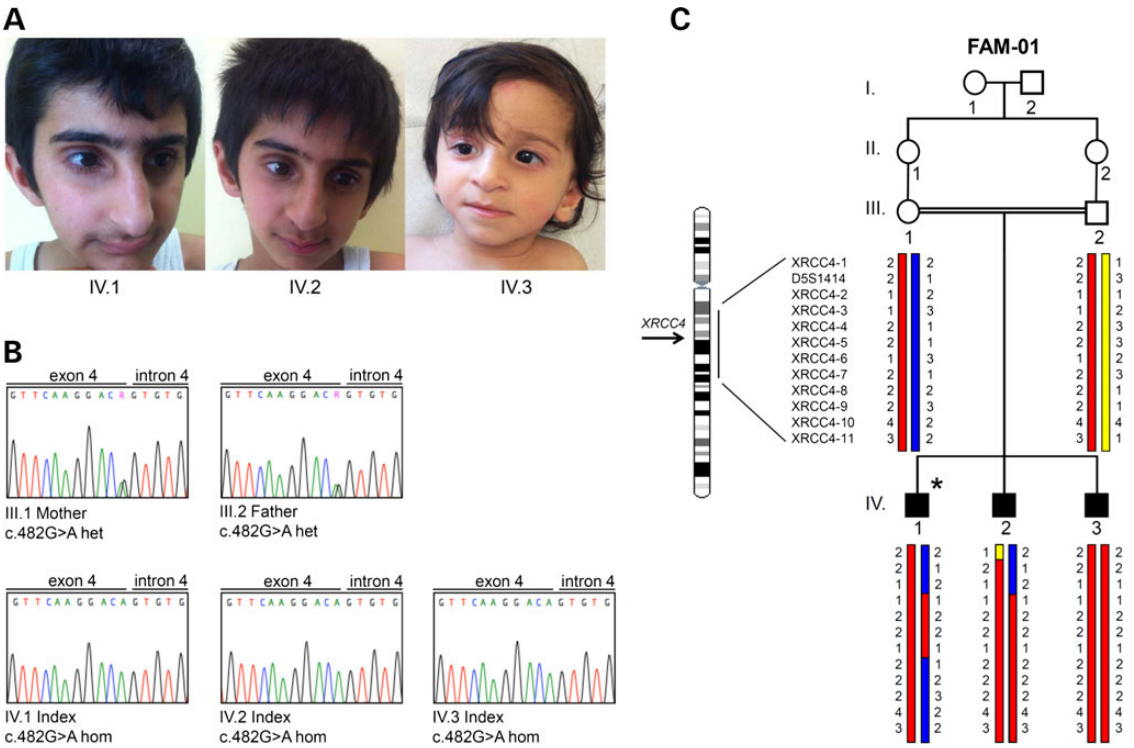

Figure 1. Clinical and molecular characterization of the Turkish family FAM-01. (**A**) Facial characteristics of affected siblings IV.1, IV.2 and IV.3 presenting with primary microcephaly, long and prominent nose, and mild hypotelorism and synophrys in individuals IV.1 and IV.2. (**B**) Electropherograms of the identified *XRCC4* mutation confirmed the homozygous missense mutation, c.482G>A, in *XRCC4* in all affected siblings while both parents were heterozygous carriers. (**C**) Pedigree of the consanguineous Turkish family FAM-01 and haplotypes of 12 microsatellite markers surrounding *XRCC4* on chromosome 5. Chromosomal location of *XRCC4* is depicted by black arrow. All three siblings are affected (solid symbols) while both parents are unaffected (white symbols). Asterisk indicates index patient IV.1, who was subjected to whole-exome sequencing.

subsequent Sanger sequencing of PCR fragments (Fig. 3). In contrast to wild-type cDNA, we observed three major *XRCC4* transcripts from cDNA of the index patient IV.1: (i) a major transcript generated by complete skipping of exon 4 of *XRCC4* predicted to cause a frameshift and premature truncation of the protein (p.Phe106Ilefs*1), (ii) a minor transcript generated by complete skipping of exons 3 and 4 of *XRCC4*, also predicted to cause a frameshift and premature truncation of XRCC4 protein (p.Val47Aspfs*5) and (iii) a correctly spliced minor transcript carrying the p.Arg161Gln missense mutation. Both, deletion of exon 4 and skipping of exons 3 and 4 are predicted to result in a frameshift and premature protein truncation deleting large, highly conserved parts of the protein suggesting most likely complete loss of XRCC4 protein function for these two aberrant transcripts.

To further investigate the impact of the c.482G>A mutation on protein function and stability, we analyzed the expression of XRCC4 in primary fibroblasts established from index patient IV.1 of family FAM-01 (hereinafter referred to as *XRCC4*-fibroblasts) and from an age- and sex-matched healthy control individual. Western blot analysis demonstrated a severe reduction of full-length XRCC4 protein in *XRCC4*-fibroblasts compared with wild-type cells, consistent with the results obtained by RT–PCR analysis (Fig. 4A). Still, we also detected a faint band of corresponding size to wild-type XRCC4, which most probably represents the full-length XRCC4 carrying the p.Arg161Gln missense mutation. Furthermore, we did not observe any protein expression of the truncated XRCC4 forms in patient fibroblasts implying protein instability and complete loss of function of these truncated XRCC4 variants.

For detailed analysis of protein stability, we cloned wild-type and mutant *XRCC4* cDNA mimicking the most prominent transcript identified in the index patient IV.1 (family FAM-01) (XRCC4 p.Phe106Ilefs*1) into a mammalian expression vector with a C-terminal FLAG tag. Whereas transfection of HEK293T cells with wild-type *XRCC4* resulted in detection of recombinant, FLAG-tagged protein, we were not able to detect expression of the p.Phe106Ilefs*1 mutant protein (Fig. 4B). Moreover, treatment of cells with MG-132, a potent inhibitor of the ubiquitin-dependent proteasome system, did also not result in detection of residual mutant protein, which suggests that either no truncated XRCC4 protein is expressed or different pathways are utilized for its immediate degradation.

XRCC4-fibroblasts are hypersensitive to DSB-inducing agents

XRCC4 is a ubiquitously expressed protein that is involved in the repair of DNA DSBs. Together with LIG4, XRCC4 forms a complex which plays a crucial role in the final ligation step of DNA DSB repair via NHEJ (13–16). To further characterize the effects of XRCC4 deficiency on DNA damage response pathways and DNA repair, we treated *XRCC4*-fibroblasts either with UV light [in order to induce nucleotide excision repair (NER) mediated DNA repair], or etoposide (to activate DNA DSB repair) and monitored the activation of H2AX, which occurs rapidly after exposure to DNA damage and represents a sensitive marker for DNA damage and subsequent repair of DNA lesions (17). Whereas we could not observe any differences in the activation of H2AX after irradiation of

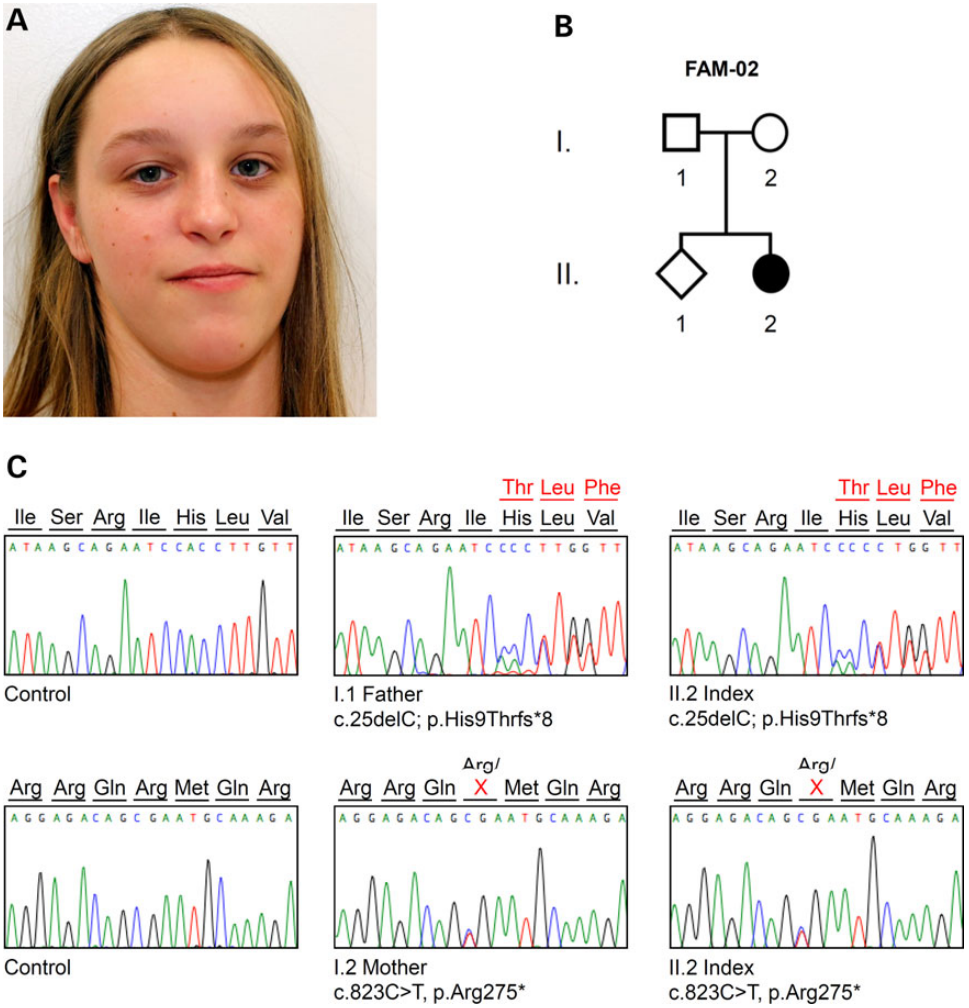

Figure 2. Clinical and molecular characterization of index patient II.2 of the Swiss family FAM-02. (**A**) Facial characteristics of index patient II.2 presenting with primary microcephaly, long face with prominent chin, high nasal bridge, and mild strabism. (**B**) Pedigree of the non-consanguineous Swiss family FAM-02. (**C**) Electropherograms of identified compound heterozygous *XRCC4* mutations, c.25delC and c.823C>T, compared with wild-type (Control) sequences and heterozygous carrier sequences of the father (I.1), mother (I.2).

wild-type and patient cells with UV light, *XRCC4*-fibroblasts showed a marked sensitivity to etoposide treatment and responded with hyperphosphorylation of H2AX (Fig. 5A). To analyze the cellular response to DNA DSBs in detail, we treated cells with the radiomimetic chemical zeocin, which belongs to the bleomycin family of antibiotics and has been shown to specifically induce DNA DSBs. Treatment of *XRCC4*-fibroblasts with low doses of zeocin resulted in a significant activation of H2AX in *XRCC4*-fibroblasts, whereas wild-type cells did not show any H2AX activation (Fig. 5B). Moreover, treatment with higher concentrations of zeocin induced hyperphosphorylation of H2AX in *XRCC4*-fibroblasts comparable to that seen after etoposide treatment. We next analyzed the activation of H2AX by flow cytometry in detail and observed an increased and prolonged H2AX activation after etoposide treatment in *XRCC4*-fibroblasts indicating that disruption of XRCC4 reduces DNA DSB repair ability and pointing towards a very critical function of XRCC4 during these processes (Fig. 5C).To analyze the formation and repair of DNA DSBs in more detail, we performed a neutral comet assay and quantified the amount of DSBs in wild-type and *XRCC4*-fibroblasts after etoposide treatment. In the the neutral comet assay the extension of tailing, measured by the tail moment, correlates with the appearance of DSBs. Using this method we were able to assess the amount of DSBs and thereby the efficiency of DSB repair in *XRCC4*-fibroblasts. Interestingly, we did not observe any differences in the tail moment comparing untreated wild-type and *XRCC4*-cells suggesting that either residual XRCC4 p.Arg161Gln is sufficient to handle low levels of DSBs produced by normal cellular processes or that these lesions can be repaired independently of XRCC4. However, after etoposide treatment, the occurrence of DSBs in *XRCC4*-fibroblasts was significantly higher compared with wild-type cells (Fig. 6A and B) confirming the important role of fully functional XRCC4 in the repair of these DNA lesions.

DNA DSBs are one of the most cytotoxic forms of DNA lesions and the repair of DSBs is crucial for the maintenance of genomic integrity. If unrepaired, DSBs can induce apoptosis and, thereby, give rise to increased cell death. In order to investigate the impact of unrepaired DSBs on cell viability and survival, we analyzed the cytotoxicity of exposure to etoposide by MTT assay (Fig. 6C). We observed a significantly higher cytotoxicity in *XRCC4*-fibroblasts compared with wild-type cells suggesting that functional impairment of XRCC4 does not only directly affect DSB repair, but furthermore results in the induction of cell death if DNA lesions remain unrepaired.

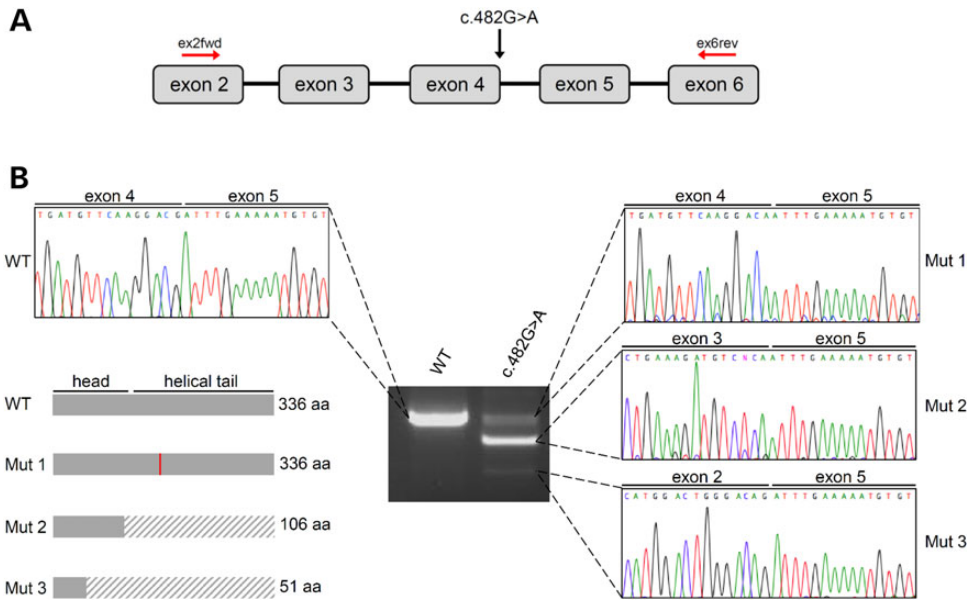

Figure 3. RT–PCR analysis of *XRCC4* transcripts. (**A**) Schematic representation of the amplified region of *XRCC4* cDNA and locations of primers used for the amplification. The black arrow indicates the position of the c.482G>A mutation in exon 4. (**B**) RT–PCR analysis of *XRCC4* in individual IV.1 showed three different transcripts (Mut 1–3): two alternative transcripts of smaller size, and one transcript of corresponding size compared with WT (Mut 1). Sequencing of the WT and Mut 1–3 RT–PCR products determined the exon composition of all transcripts showing that the c.482G>A mutation mainly leads to alternatively spliced *XRCC4* pre-mRNA. Lower left panel: Functional consequences of impaired *XRCC4* pre-mRNA splicing on protein level. The main splicing product characterized by exon 4 skipping induces a frameshift and premature protein truncation (Mut 2, p.Phe106Ilefs*1). A second splicing product generated by skipping of exons 3 and 4 is predicted to cause a truncated protein of 51 amino acids (Mut 3, p.Val47Aspfs*5). Additionally, we observed a correctly spliced *XRCC4* transcript resulting in translation of a mutant XRCC4 protein carrying a missense mutation (Mut 1, p.Arg161Gln). The red line indicates the position of the substituted amino acids in XRCC4 (grey box). Hatched areas represent the missing parts in the truncated proteins.

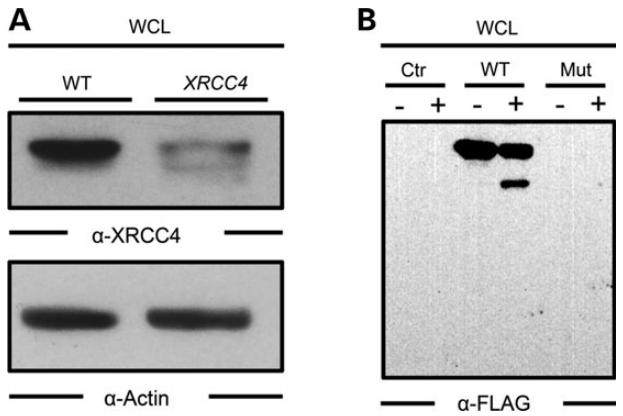

Figure 4. The c.482G>A mutation in *XRCC4* alters protein stability. (**A**) Upper panel: western blot analysis of XRCC4 expression in wild-type (WT) and patient fibroblasts (*XRCC4*) established from individual IV.1 revealed a strong reduction in XRCC4 expression in cells carrying the c.482G>A mutation. No truncated forms of XRCC4 were detectable in patient cells. Lower panel: equal protein loading was confirmed by re-probing of the membrane with antibodies against actin. (**B**) HEK293T cells were transfected with FLAG-tagged wild-type XRCC4 (WT), XRCC4 p.Phe106Ilefs*1 (Mut) or empty vector as control (Ctr). Cells were either treated with the proteasome inhibitor MG-132 (+) or left untreated (–). Cells were lysed, and whole cellular lysates (WCL) were subjected to western blot analysis with anti-FLAG antibodies. No truncated form of XRCC4 could be detected before or after treatment of cells with MG-132.

Discussion

Here, we show that mutations in XRCC4 are associated with primary microcephaly, facial dysmorphism and short stature. Moreover, we show that the identified mutations mainly lead to premature protein truncation and protein instability resulting in hypersensitivity to DNA DSBs, retarded DSB repair and increased cell death in *XRCC4*-fibroblasts.

XRCC4 is an essential factor in NHEJ, which is one of two major pathways for the repair of DNA DSBs in mammalian cells (1). It can directly bind to DNA and it forms a stable complex together with the DNA ligase IV, which localizes to the broken DNA ends. XRCC4 stimulates and influences the joining activity of LIG4 directly and indirectly due to its interaction and recruitment of NHEJ1, an additional protein regulating LIG4 activity (1,8,18,19).

Previous studies indicate that NHEJ is the predominant pathway for the repair of DNA DBSs in differentiated neuronal cells (20). As HR relies on the presence of suitable homologous templates like sister chromatids, NHEJ is the only appropriate pathway to repair DSBs in non-dividing, differentiated neurons. Additionally, neurons display a high metabolic rate probably thereby giving rise to an increased production of reactive metabolites like ROS, which, for example, can cause DNA damage. An efficient DNA repair machinery is therefore important to repair these kinds of lesions. Complete knockout of NHEJ key factors leads to extensive cell death in neuronal tissue resulting in embryonic lethality as shown in different animal models. In accordance with these observations patients with recessive mutations in *LIG4*, *NHEJ1* or *PRKDC* present, e.g. with severe primary microcephaly often associated with seizures, simplified gyral pattern and short stature (7,8,10,11,21,22). Consistent with these studies, all patients presented here showed a typical NHEJ-related phenotype defined by marked microcephaly, typical facial dysmorphism, developmental delay and mild intellectual disability. Interestingly, we did not observe any immunodeficiency in any of the affected individuals, which is in line with a previously reported patient presenting with microcephaly and

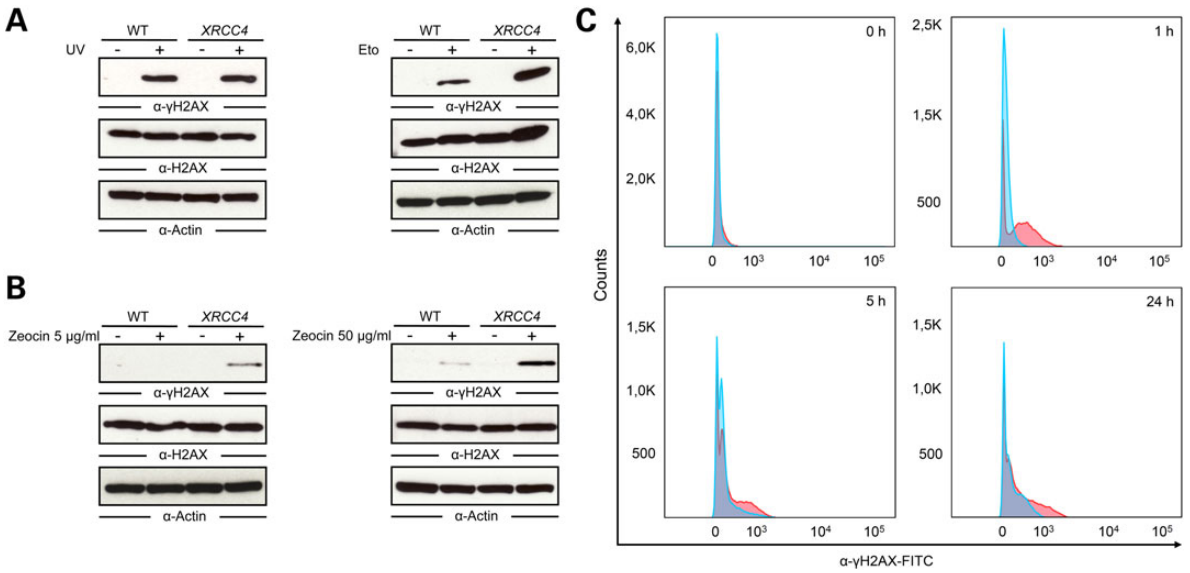

Figure 5. XRCC4-fibroblasts are hypersensitive to DSB-inducing agents. (**A**) Western blot analysis of UV- and etoposide-induced phosphorylation of H2AX (Ser139). XRCC4-fibroblasts (XRCC4) and wild-type cells (WT) were treated with UV-C or etoposide, lysed and subjected to western blot analysis. Equal protein loading was confirmed by re-probing of the membrane with antibodies against H2AX and actin. (**B**) Western blot analysis of zeocin-induced phosphorylation of H2AX (Ser139). XRCC4-fibroblasts (XRCC4) and wild-type cells (WT) were treated with 5 µg/ml (left panel) or 50 µg/ml (right panel) zeocin, lysed and subjected to western blot analysis. Equal protein loading was confirmed by re-probing of the membrane with antibodies against H2AX and actin. (**C**) FACS analysis of wild-type (blue) and XRCC4-fibroblasts (red) after exposure to etoposide for 1 h. Cells were harvested 1, 5 and 24 h after treatment. Untreated cells (0 h) were used as controls. While untreated wild-type and XRCC4-fibroblasts do not show differences in basal H2AX activation, treatment with etoposide induced a significant increase in γH2AX levels in XRCC4-fibroblasts compared with wild-type cells.

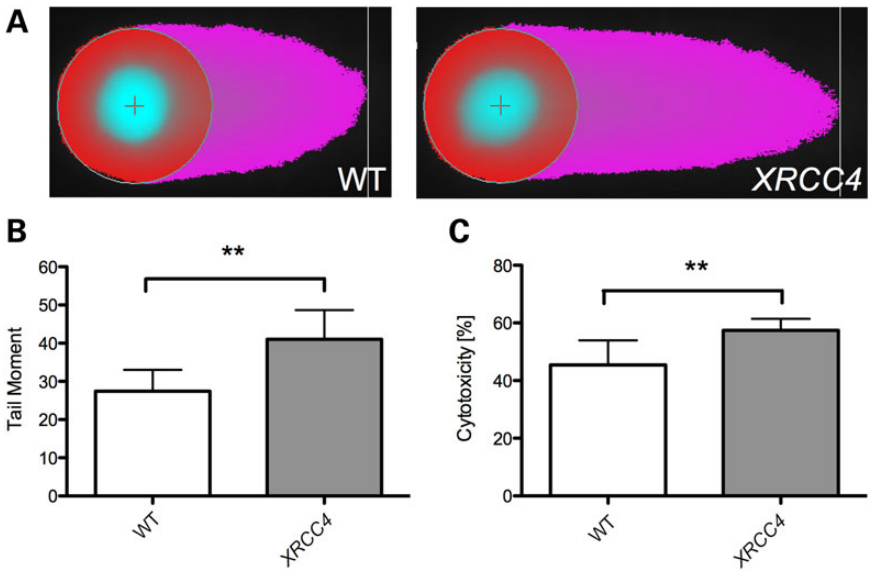

Figure 6. The c.482G>A mutation in XRCC4 impairs DSB repair. (**A**) Representative images of wild-type (WT) and XRCC4-fibroblasts (XRCC4) analysed by neutral comet assay. (**B**) Quantification of tail moments in wild-type (WT) and XRCC4-fibroblasts (XRCC4) after treatment with etoposide for 1 h, followed by a repair period of 1 h and subsequent analysis via neutral comet assay. The tail moment (|percentage of DNA content in tail| × |tail length|) was used to evaluate DNA damage and repair efficiency. The displayed data indicate that the tail moment is significantly increased in XRCC4-fibroblasts compared with wild-type cells (*P*-value = 0.0092). Statistical significance was analysed using paired Student's *t*-test. Error bars represent SD. $n = 3$. **P-value < 0.01. (**C**) MTT assay of wild-type (WT) and XRCC4-fibroblasts (XRCC4) after treatment with etoposide for 1 hour and analysis 72 h later. Untreated cells were used throughout the experiments as controls. Three different wild-type cell lines were analysed in triplicates during each experiment and values were pooled afterwards for graphical presentation. The cytotoxicity is increased in XRCC4-fibroblasts compared with wild-type cells (*P*-value = 0.0072). Statistical significance was analysed using paired Student's *t*-test. Error bars represent SD. $n = 4$. **P-value < 0.01.

short stature due to a missense alteration in XRCC4 (12). However, it remains unclear why mutations in XRCC4 do not cause any observable immunological defects as it is well known that NHEJ plays an essential role in V(D)J-recombination during B- and T-cell maturation, and mutations in other key factors of NHEJ like *LIG4*, *PRKDC* and *DCLRE1C* lead to moderate-to-severe

immunodeficiency (6–11). In contrast to the phenotype observed in humans with mutations in *XRCC4*, examination of fetal thymi isolated from *Xrcc4* knockout mice shows markedly reduced size, and both, B and T-cell development is arrested in early stages in these animals (22). It remains possible that an immunological phenotype might occur later in life in patients with *XRCC4* mutations.

Our analysis of the functional consequences of the c.482G>A mutation identified in family FAM-01 showed that this substitution in exon 4 most abundantly induces aberrant XRCC4 splicing resulting in the generation of differently truncated XRCC4 variants. However, we also observed a small portion of correctly spliced transcript carrying the p.Arg161Gln missense mutation in XRCC4. Thus, the identified mutation in *XRCC4* is likely hypomorphic. Still, we can only speculate, if the residual full-length protein carrying the p.Arg161Gln mutation is functional or not. The argenine at position 161 is not very well conserved and therefore, some residual XRCC4 activity is likely to be present, which possibly explains the phenotypic difference between the knockout mouse model and the patients presented in this study. In the index patient II.2 of family FAM-02, we identified compound heterozygous truncating mutations, c.25delC and c.823C>T, in *XRCC4*. The paternally inherited c.25delC deletion is predicted to cause an early frameshift at p.His9 and most likely a complete loss of protein function. The c.823C>T mutation, which was inherited by the mother, induces a premature protein truncation at the very end of the protein (p.Arg275*). Especially, the evolutionarily highly conserved LIG4-binding site in XRCC4 is still present, possibly enabling at least partial functionality of the XRCC4 p.Arg275* protein.

Notably, it has been shown that LIG4- and PRKDC-deficient patients also exhibit hypomorphic mutations in *LIG4* and *PRKDC*, respectively, which provide residual protein function (6,7,10,11). Like *Xrcc4*, knockout of *Lig4* in mice is embryonically lethal suggesting that complete loss of function mutations of *LIG4* and *XRCC4* may not be compatible with life in humans (21–23). Moreover, biochemical and cellular studies revealed that mutations identified in *LIG4* vary in their impact on LIG4 enzymatic activity with earlier truncating mutations being more severe than mutations at the C-terminal end of LIG4 (24–27). Interestingly, these observations correlate with the disease severity observed in humans with 'early' truncating mutations having the most severe phenotype, while truncating mutations at the C-terminus of LIG4 cause a less severe phenotype (11).

Finally, at a cellular level, we could show that mutations in *XRCC4* induce a marked sensitivity to DSB-inducing agents, and that DSB repair occurs at a lower efficiency compared with wild-type cells. Consistent with our results, previous studies using XRCC4- and *LIG4*-knockout cell lines revealed similar results. LIG4- and XRCC4-deficient cells exhibited an increased sensitivity to ionizing radiation or treatment with DSB-inducing chemicals resulting in slower kinetics of DSB repair and drastically reduced survival after treatment (22,28,29). Interestingly, in line with our observation, UV-C induced DNA damage response was not altered in cells lacking XRCC4 (30).

In summary, our data provide evidence that hypomorphic, autosomal recessive mutations in *XRCC4* cause a NHEJ-related syndrome defined by facial dysmorphism, primary microcephaly and short stature, but without immunological phenotype. Moreover, we observed that XRCC4-deficiency leads to hypersensitivity to DSB-inducing agent and defective DSB repair, which results in increased cell death after exposure to genotoxic agents.

Materials and Methods

Subjects

The study was performed in accordance with the Declaration of Helsinki protocols and was approved by the Ethic Committee of the University Hospital Cologne, Germany. Peripheral blood samples from the affected children and parents were collected after written informed consent was obtained according to the protocols approved by the participating institutions. Written consent for publication of the photographs was given. DNA from participating family members was extracted from peripheral blood lymphocytes by standard extraction procedures.

NGS-based sequencing approaches

Whole-exome sequencing was performed on the index patient IV.1 of family FAM-01. Exonic and adjacent intronic sequences were enriched from genomic DNA using the NimbleGen SeqCap EZ Human Exome Library v2.0 enrichment kit and were run on an Illumina HiSeq2000 sequencer by the Cologne Center for Genomics (CCG). Data analysis and filtering of mapped target sequences was performed with the 'Varbank' exome and genome analysis pipeline v.2.1 (CCG) and data were filtered for high-quality (coverage of more than six reads, a minimum quality score of 10), rare (MAF < 0.5%) autosomal recessive variants. A disease-associated gene panel was performed on DNA of the index patient II.2 of family FAM-02 using the TruSight™ One Sequencing Panel (4813 genes included, Illumina) with paired-end sequencing (TruSeq Rapid Kit, 150 Fwd-150 Rev) on a Illumina HiSeq System. The average depth of coverage was ×145 and about 94.2% of the targeted bases were assessed by ≥20 independent sequence reads.

Mutation screening

Variants identified by NGS-based approaches were amplified from DNA of the index patients and PCR products were sequenced by BigDye Terminator method on an ABI PRISM® 3100 Avant Genetic Analyzer (Life Technologies, Germany). Identified mutations were re-sequenced in independent experiments and tested for co-segregation within the families.

Microsatellite marker analysis

Microsatellite markers of three affected individuals of family FAM-01 (IV.1, IV.2 and IV.3) and their parents (III.1 and III.2) were genotyped using the ABI PRISM® 3100 Avant Genetic Analyzer and GeneScan® 3.7 software (Life Technologies, Germany). Primer sequences to amplify specific markers were taken from the UCSC genome browser (http://www.genome.ucsc.edu) and primers were designed according to the reference sequences. Primers are available on request.

cDNA analysis

RNA was extracted from wild-type and fibroblasts derived from index patient IV.1 of family FAM-01 using the RNeasy Mini Kit (Qiagen, Germany) and following manufacturer's instructions. RNA was reverse transcribed using the RevertAid™ First Strand cDNA Synthesis Kit (Thermo Fisher Scientific, Germany). Primers were designed according to the XRCC4 reference sequence and amplified PCR products were separated on an agarose gel, purified using the QIAquick Gel Extraction Kit (Qiagen, Germany) and prepared for sequence analysis.

Generation of wild-type and mutant XRCC4 expression constructs

Generation of wild-type (RefSeq NM_022406; NP_071801) and mutant XRCC4 expression plasmid containing coding sequences of human XRCC4 with an additional, C-terminal FLAG tag was amplified by RT–PCR from isolated fibroblast RNA and cloned into the pcDNA3.1 expression vector (Life Technologies, Germany). All cDNA sequences were confirmed by Sanger sequencing.

Cell lines and cell cultures

HEK293T cells and primary fibroblast cell lines established from patient VI.1 of family FAM-01 were cultured in Dulbecco's modified Eagle medium (DMEM, Gibco) supplemented with 10% fetal calf serum (FCS, Gibco), and antibiotics. For H2AX activation, cells were either irradiated with 100 J/m^2 UV-C or treated with 50 µM etoposide (Sigma-Aldrich, USA), 5 µg/ml or 50 µg/ml zeocin (Invivogen, France) for 1 h. Drugs were then washed out, fresh media was added and cells were incubated for the indicated times and then subjected to western blot or FACS analysis. HEK293T cells were transfected with 2 µg of each plasmid by using Fugene® HD Transfection reagent (Promega, Germany) following manufacturer's instructions and cells were solubilized 24 h post-transfection.

Protein isolation and analysis

Cells were solubilized by using ice-cold RIPA buffer [10 mM Tris, pH: 8.0; 150 mM NaCl; 1 mM EDTA; 10 mM NaF; 1 mM Na_3VO_4; 10 µM Na_2MoO_4; 1% NP-40; protease inhibitors P 2714 (Sigma-Aldrich, USA)]. The total protein concentration of extracts was determined using the BCA Protein Assay Kit (Thermo Fisher Scientific, USA). 13–25 µg of total cell lysates were separated by 4–12% SDS–PAGE (Invitrogen, Germany) and blotted onto nitrocellulose membranes (GE Healthcare, Germany). Protein detection was performed using phospho-specific antibodies to γH2AX (Ser139) (Cell Signaling Technology, USA). Antibodies to H2AX were purchased from Calbiochem (USA). Anti-β-Actin, anti-FLAG and anti-XRCC4 antibodies were purchased from Sigma-Aldrich. Secondary antibodies conjugated to peroxidase (Santa Cruz Biotechnology Inc., USA) were used and blots were developed using an enhanced chemiluminescence system, ECL Plus (GE Healthcare), followed by detection on autoradiographic films.

Neutral comet assay

Neutral comet assay was performed as described previously (31). In brief, cells were incubated with 50 µM etoposide (Sigma-Aldrich, USA) for 1 h, washed once with PBS and incubated for 1 h to enable DNA repair. Cells were harvested in PBS and diluted to 2×10^4 cells/ml. Frosted-end microscope slides were pre-coated with 1% low-gelling-temperature agarose (LGTA). Four hundred microliters of cell suspension was mixed with 1 ml pre-heated 1% LGTA, pipetted on pre-coated slides and air-dried for 2 min. Slides were submerged in N1 buffer [2% sarkosyl, 0.5 M Na_2EDTA, 0.5 mg/ml proteinase K (pH 8)] and incubated for 18–20 h at 37°C followed by three washing steps with N2 buffer [90 mM Tris buffer, 90 mM boric acid, 2 mM Na_2EDTA (pH 8.5)] for 30 min at room temperature. Samples were submerged in an electrophoresis chamber containing N2 buffer and a voltage of 1.4 V/cm was applied for 25 min. Slides were washed with distilled water and incubated in 2.5 µg/ml propidium iodide (Sigma-Aldrich, USA) in distilled water for 20 min. Finally, samples were washed with distilled water and stored until analysis in a light tight box at 4°C. Comets were visualized with the IX81 microscope (Olympus, Germany) and an average comet tail moment (|percentage of DNA content in tail| × |tail length|) was calculated for at least 70 nuclei per slide using the CaspLab software (32).

MTT assay

Wild-type and XRCC4-fibroblasts were either stressed with 75 µM etoposide (Sigma-Aldrich, USA) for 1 h or remained untreated. Seventy-two hours after treatment, cells were incubated at 37°C for 2 h in 5 mg/ml 3-(4,5-dimethylthiazol-2-yl)-2,5-diphenyltetrazolium bromide (Sigma-Aldrich, USA) in PBS. The supernatant was replaced by DMSO (AppliChem, Germany) and plates were shaken at 225 rpm and 37°C for 5 min. The readout was performed by using the TECAN Safire 2 microplate reader (TECAN, Germany) at 595 nm. The percentage of cytotoxicity was calculated as described previously (33) and each measurement was performed in triplicates with three different wild-type fibroblast cell lines and fibroblast cells established from index patient IV.1.

FACS analysis

Untreated or etoposide treated cells were harvested by trypsinization, washed with 1% BSA/PBS and subsequently PBS, fixed in 70% ethanol and stored at −20°C. For staining, cells were rehydrated in 1% BSA and 1% Triton X-100 in PBS, incubated for 10 min on ice and afterwards for 1 h in 1% powdered milk/PBS at room temperature. Samples were incubated for 2 h with anti-γH2AX (Ser139) antibodies (Cell Signaling Technology, USA), subsequently washed with PBS, monitored on a FACSCanto flow cytometer (Becton Dickinson, USA) and analyzed with FlowJo (Tree Star, USA).

Web Resources

The URLs for data presented herein are as follows: ENSEMBL (accessed February 2015), http://www.ensembl.org, UCSC Genome Browser (accessed February 2015), http://www.genome.ucsc.edu, Online Mendelian Inheritance in Man (OMIM) (accessed February 2015), http://www.ncbi.nlm.nih.gov/omim, PolyPhen (accessed February 2015), http://genetics.bwh.harvard.edu/pph/, Exome Variant Server (EVS) (accessed February 2015), http://evs.gs.washington.edu/EVS, Exome Aggregation Consortium (ExAC) (accessed April 2015), http://exac.broadinstitute.org/.

Acknowledgements

We are grateful to all family members that participated in this study, Esther Milz for excellent technical assistance and Karin Boss for critically reading the manuscript.

Conflict of Interest statement. None declared.

Funding

This work was supported by the German Federal Ministry of Education and Research (BMBF) by grant number 01GM1404 (E-RARE network EuroMicro) to B.W. and the E-RARE network EuroMicro to A.R.

References

1. Van Gent, D.C., Hoeijmakers, J.H. and Kanaar, R. (2001) Chromosomal stability and the DNA double-stranded break connection. *Nat. Rev. Genet.*, **2**, 196–206.
2. West, S.C. (2003) Molecular views of recombination proteins and their control. *Nat. Rev. Mol. Cell Biol.*, **4**, 435–445.
3. Mills, K.D., Ferguson, D.O. and Alt, F.W. (2003) The role of DNA breaks in genomic instability and tumorigenesis. *Immunol. Rev.*, **194**, 77–95.
4. Lieber, M.R., Ma, Y., Pannicke, U. and Schwarz, K. (2003) Mechanism and regulation of human non-homologous DNA end-joining. *Nat. Rev. Mol. Cell Biol.*, **4**, 712–720.
5. Shrivastav, M., De Haro, L.P. and Nickoloff, J.A. (2008) Regulation of DNA double-strand break repair pathway choice. *Cell Res.*, **18**, 134–147.
6. Van der Burg, M., Ijspeert, H., Verkaik, N.S., Turul, T., Wiegant, W.W., Morotomi-Yano, K., Mari, P.-O., Tezcan, I., Chen, D.J., Zdzienicka, M.Z. *et al.* (2009) A DNA-PKcs mutation in a radiosensitive T-B- SCID patient inhibits Artemis activation and nonhomologous end-joining. *J. Clin. Invest.*, **119**, 91–98.
7. Woodbine, L., Neal, J.A., Sasi, N.-K., Shimada, M., Deem, K., Coleman, H., Dobyns, W.B., Ogi, T., Meek, K., Davies, E.G. *et al.* (2013) PRKDC mutations in a SCID patient with profound neurological abnormalities. *J. Clin. Invest.*, **123**, 2969–2980.
8. Buck, D., Malivert, L., de Chasseval, R., Barraud, A., Fondanèche, M.-C., Sanal, O., Plebani, A., Stéphan, J.-L., Hufnagel, M., le Deist, F. *et al.* (2006) Cernunnos, a novel nonhomologous end-joining factor, is mutated in human immunodeficiency with microcephaly. *Cell*, **124**, 287–299.
9. Li, L., Moshous, D., Zhou, Y., Wang, J., Xie, G., Salido, E., Hu, D., de Villartay, J.-P. and Cowan, M.J. (2002) A founder mutation in Artemis, an SNM1-like protein, causes SCID in Athabascan-speaking Native Americans. *J. Immunol.*, **168**, 6323–6329.
10. O'Driscoll, M., Cerosaletti, K.M., Girard, P.M., Dai, Y., Stumm, M., Kysela, B., Hirsch, B., Gennery, A., Palmer, S.E., Seidel, J. *et al.* (2001) DNA ligase IV mutations identified in patients exhibiting developmental delay and immunodeficiency. *Mol. Cell*, **8**, 1175–1185.
11. Murray, J.E., Bicknell, L.S., Yigit, G., Duker, A.L., van Kogelenberg, M., Haghayegh, S., Wieczorek, D., Kayserili, H., Albert, M. H., Wise, C.A. *et al.* (2014) Extreme growth failure is a common presentation of ligase IV deficiency. *Hum. Mutat.*, **35**, 76–85.
12. Shaheen, R., Faqeih, E., Ansari, S., Abdel-Salam, G., Al-Hassnan, Z.N., Al-Shidi, T., Alomar, R., Sogaty, S. and Alkuraya, F.S. (2014) Genomic analysis of primordial dwarfism reveals novel disease genes. *Genome Res.*, **24**, 291–299.
13. Li, Z., Otevrel, T., Gao, Y., Cheng, H.L., Seed, B., Stamato, T.D., Taccioli, G.E. and Alt, F.W. (1995) The XRCC4 gene encodes a novel protein involved in DNA double-strand break repair and V(D)J recombination. *Cell*, **83**, 1079–1089.
14. Grawunder, U., Wilm, M., Wu, X., Kulesza, P., Wilson, T.E., Mann, M. and Lieber, M.R. (1997) Activity of DNA ligase IV stimulated by complex formation with XRCC4 protein in mammalian cells. *Nature*, **388**, 492–495.
15. Critchlow, S.E., Bowater, R.P. and Jackson, S.P. (1997) Mammalian DNA double-strand break repair protein XRCC4 interacts with DNA ligase IV. *Curr. Biol.*, **7**, 588–598.
16. Berg, E., Christensen, M.O., Dalla Rosa, I., Wannagat, E., Jänicke, R.U., Rösner, L.M., Dirks, W.G., Boege, F. and Mielke, C. (2011) XRCC4 controls nuclear import and distribution of Ligase IV and exchanges faster at damaged DNA in complex with Ligase IV. *DNA Repair (Amst.)*, **10**, 1232–1242.
17. Fernandez-Capetillo, O., Lee, A., Nussenzweig, M. and Nussenzweig, A. (2004) H2AX: the histone guardian of the genome. *DNA Repair (Amst.)*, **3**, 959–967.
18. Modesti, M., Hesse, J.E. and Gellert, M. (1999) DNA binding of Xrcc4 protein is associated with V(D)J recombination but not with stimulation of DNA ligase IV activity. *EMBO J.*, **18**, 2008–2018.
19. Ahnesorg, P., Smith, P. and Jackson, S.P. (2006) XLF interacts with the XRCC4-DNA ligase IV complex to promote DNA nonhomologous end-joining. *Cell*, **124**, 301–313.
20. Orii, K.E., Lee, Y., Kondo, N. and McKinnon, P.J. (2006) Selective utilization of nonhomologous end-joining and homologous recombination DNA repair pathways during nervous system development. *Proc. Natl Acad. Sci. USA*, **103**, 10017–10022.
21. Frank, K.M., Sekiguchi, J.M., Seidl, K.J., Swat, W., Rathbun, G. A., Cheng, H.L., Davidson, L., Kangaloo, L. and Alt, F.W. (1998) Late embryonic lethality and impaired V(D)J recombination in mice lacking DNA ligase IV. *Nature*, **396**, 173–177.
22. Gao, Y., Sun, Y., Frank, K.M., Dikkes, P., Fujiwara, Y., Seidl, K.J., Sekiguchi, J.M., Rathbun, G.A., Swat, W., Wang, J. *et al.* (1998) A critical role for DNA end-joining proteins in both lymphogenesis and neurogenesis. *Cell*, **95**, 891–902.
23. Barnes, D.E., Stamp, G., Rosewell, I., Denzel, A. and Lindahl, T. (1998) Targeted disruption of the gene encoding DNA ligase IV leads to lethality in embryonic mice. *Curr. Biol.*, **8**, 1395–1398.
24. Riballo, E., Critchlow, S.E., Teo, S.H., Doherty, A.J., Priestley, A., Broughton, B., Kysela, B., Beamish, H., Plowman, N., Arlett, C. F. *et al.* (1999) Identification of a defect in DNA ligase IV in a radiosensitive leukaemia patient. *Curr. Biol.*, **9**, 699–702.
25. Riballo, E., Doherty, A.J., Dai, Y., Stiff, T., Oettinger, M.A., Jeggo, P.A. and Kysela, B. (2001) Cellular and biochemical impact of a mutation in DNA ligase IV conferring clinical radiosensitivity. *J. Biol. Chem.*, **276**, 31124–31132.
26. Marchetti, C., Walker, S.A., Odreman, F., Vindigni, A., Doherty, A.J. and Jeggo, P. (2006) Identification of a novel motif in DNA ligases exemplified by DNA ligase IV. *DNA Repair (Amst.)*, **5**, 788–798.
27. Girard, P.-M., Kysela, B., Härer, C.J., Doherty, A.J. and Jeggo, P. A. (2004) Analysis of DNA ligase IV mutations found in LIG4 syndrome patients: the impact of two linked polymorphisms. *Hum. Mol. Genet.*, **13**, 2369–2376.
28. Adachi, N., Ishino, T., Ishii, Y., Takeda, S. and Koyama, H. (2001) DNA ligase IV-deficient cells are more resistant to ionizing radiation in the absence of Ku70: Implications for DNA double-strand break repair. *Proc. Natl Acad. Sci. USA*, **98**, 12109–12113.
29. Woodbine, L., Gennery, A.R. and Jeggo, P.A. (2014) The clinical impact of deficiency in DNA non-homologous end-joining. *DNA Repair (Amst.)*, **16**, 84–96.
30. Delacôte, F., Han, M., Stamato, T.D., Jasin, M. and Lopez, B.S. (2002) An xrcc4 defect or Wortmannin stimulates homologous recombination specifically induced by double-strand breaks in mammalian cells. *Nucleic Acids Res.*, **30**, 3454–3463.
31. Olive, P.L. and Banáth, J.P. (2006) The comet assay: a method to measure DNA damage in individual cells. *Nat Protoc*, **1**, 23–29.
32. Końca, K., Lankoff, A., Banasik, A., Lisowska, H., Kuszewski, T., Góźdź, S., Koza, Z. and Wojcik, A. (2003) A cross-platform public domain PC image-analysis program for the comet assay. *Mutat. Res.*, **534**, 15–20.
33. Yarandi, N., Zali, H., Shokrgozar, M.A., Mansouri, V., Shahani, M., Rostami, A. and Heidari, S. (2010) Study of apoptosis inducing activity of calprotectin on fibroblast cell. *J. Paramed. Sci.*, **1**, 9–15.